CHAPTER 6

DISCUSSIONS ON THE PROPOSED MODEL

6.1 Discussions on the Existing Models for the Predictions of NVG Point, True Quality, Void Fraction and Drag Coefficient

Accurate CHF computation from the present model relies greatly on the accurate prediction of some important and basic items, such as the NVG point, true quality and the void fraction. This section first gives analysis and comparisons among the existing models for the NVG point, true quality and void fraction calculations, aiming to get a base for appropriate model adoption in the present CHF prediction procedure. Sensitivity studies comparing the model's predictions by using correlations for the NVG point, true quality, void fraction and drag coefficient are also carried out.

6.1.1 The NVG Point

6.1.1.1 Comparisons for the NVG Models

The NVG (ΔT_d) point is the base for the true quality and the void fraction calculation. Under a certain condition, too low (high) ΔT_d prediction means the calculated NVG point is more difficult (easy) to reach than actual and would result in a too low (high) true quality and void fraction calculation, which in turn, results a too high (low) CHF prediction. For the NVG point, three correlations are well known. They are:

(1) Levy Model (1967)

In Levy 1967 model, a force balance was used to establish the criterion for the NVG point. Once the size of the bubble at incipient departure is known, the subcooling ΔT_d is calculated by assuming: firstly, the single-phase temperature profiles in the liquid and secondly, the fluid temperature at a distance corresponding to the departure bubble radius equals to the saturation temperature T_{SAT}. Then,

$$\Delta T_d = q_m \left(\frac{1}{h_l} - \frac{T_B^+}{C_{pf} \rho_f u^*} \right) \qquad (6\text{-}1)$$

where h_l is Dittus-Boelter's liquid heat transfer coefficient. T_B^+ is calculated from

$$\begin{cases} T_B^+ = \mathrm{Pr}_f Y_B^+ & 0 \le Y_B^+ \le 5 \\ T_B^+ = 5\left\{ \mathrm{Pr}_f + \ln\left[1 + \mathrm{Pr}_f \left(\frac{Y_B^+}{5} - 1 \right) \right] \right\} & 5 \le Y_B^+ \le 30 \\ T_B^+ = 5\left[\mathrm{Pr}_f + \ln\left(1 + 5\,\mathrm{Pr}_f\right) + 0.5 \ln\left(\frac{Y_B^+}{30} \right) \right] & Y_B^+ > 30 \end{cases} \qquad (6\text{-}2)$$

with $Y_B^+ = \frac{Y_B u^* \rho_f}{\mu_f}$ (6-3) $u^* = \sqrt{\tau_w / \rho_f}$ (6-3a)

$$Y_B = 0.015\left(\frac{\sigma D}{\tau_w}\right)^{1/2} \quad (6\text{-}4) \quad \tau_w = \frac{fG^2}{8\rho_f} \quad (6\text{-}4a)$$

(2) Saha-Zuber Model (1974)

For Peclet number less than 70000, the local subcooling at NVG point is found independent of flow velocity. The region is considered as thermal controlled region. For Peclet number greater than 70000, Stanton number at NVG point is found to be a constant. Bubble departure is hydrodynamic induced and occurs at a fixed Stanton number of 0.0065. ΔT_d is so calculated from:

$$\begin{cases} Nu = \dfrac{q_m D}{k_f \Delta T_d} = 455 & Pe \le 70000 \\ St = \dfrac{q_m}{G C_{pf} \Delta T_d} = 0.0065 & Pe > 70000 \end{cases} \quad (6\text{-}5)$$

(3) Ahmad Model (1970)

ΔT_d is simply calculated from:

$$\Delta T_d = q_m / h_{l\text{-}A} \quad (6\text{-}6)$$

where $h_{l\text{-}A}$ is correlated as:

$$h_{l\text{-}A} = 2.44\frac{k_f}{D}\left(\frac{GD}{\mu_f}\right)^{1/2}\left(\frac{C_{pl,T_d}\mu_f}{k_f}\right)^{1/3}\left(\frac{H_{lin}}{H_f}\right)^{1/3}\left(\frac{H_{fg}}{H_f}\right)^{1/3} \quad (6\text{-}7)$$

In the following, heat flux q_m, mass velocity G, pressure P, inner diameter D, heated length L and inlet temperature T_{in} effects on ΔT_d are compared among the above three models.

6.1.1.1 1 The Mass flux G Effect on the ΔT_d

The three NVG models all show the ΔT_d is inversely proportional to the mass flux to some power as $\Delta T_{d\text{-Levy}}$ nearly proportional to $G^{-0.8}$, $\Delta T_{d\text{-Ahmad}}$ proportional to $G^{-0.5}$ and $\Delta T_{d\text{-Saha}}$ proportional to G^{-1} when Pe number higher than 70000 (no relation with G when Pe number is lower than 700000). A representative G effects on ΔT_d are shown in Fig.6-1. The broken line represents the result from the Ahmad model. The Levy ΔT_d is found being affected by the mass flux most significantly, especially at low mass flux condition. Under the condition shown in the figure, the Levy ΔT_d at low mass flux condition is more than 2 times

higher than the ΔT_d from the Ahmad model. At low mass flux condition, the Levy NVG model is considered giving too high ΔT_d prediction and therefore is not recommended. At low mass flux condition, the using of Levy NVG model would cause the too low CHF prediction results.

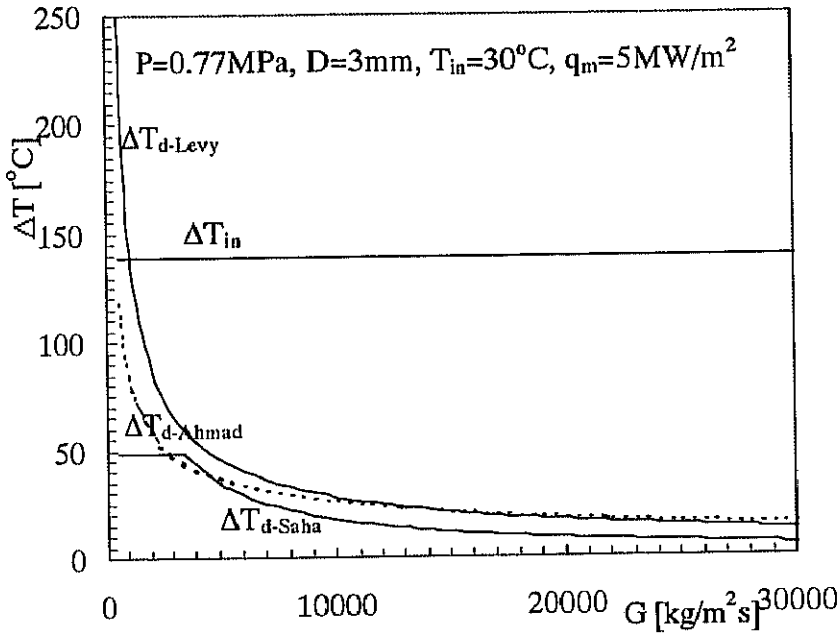

Fig.6-1 Mass Flux G Effect on the ΔT_d

6.1.1.1 2 Heat flux q_m Effect on ΔT_d

The three models predict a similar effect of the heat flux q_m on the ΔT_d. The ΔT_d is an increasing function of the heat flux. Representative q_m effect on the ΔT_d is shown in fig.6-2.

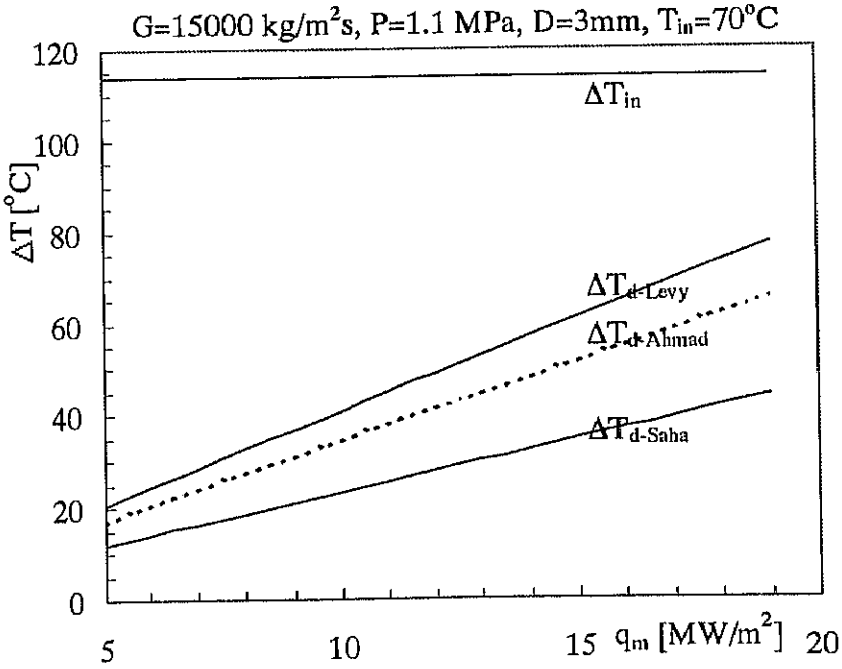

Fig.6-2 Heat Flux q_m Effect on the ΔT_d

6.1.1.1 3 The Pressure P Effect on the ΔT_d

The Pressure P shows doing different effects on the NVG point in different model. As shown in fig.6-3, except $\Delta T_{d\text{-}Ahmad}$ is an increasing function, $\Delta T_{d\text{-}Levy}$ and $\Delta T_{d\text{-}Saha}$ generally decreases with the increases of the pressure, especially at high pressure. Although it is still difficult to judge which tendency is right, from the CHF prediction results, the Ahmad model seems give best NVG prediction at high-pressure condition.

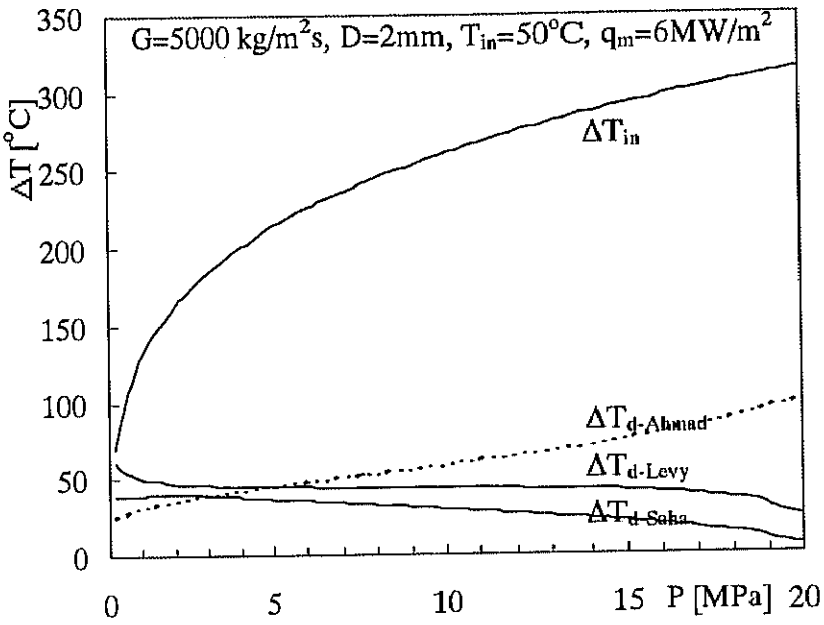

Fig.6-3 Pressure P Effect on the ΔT_d

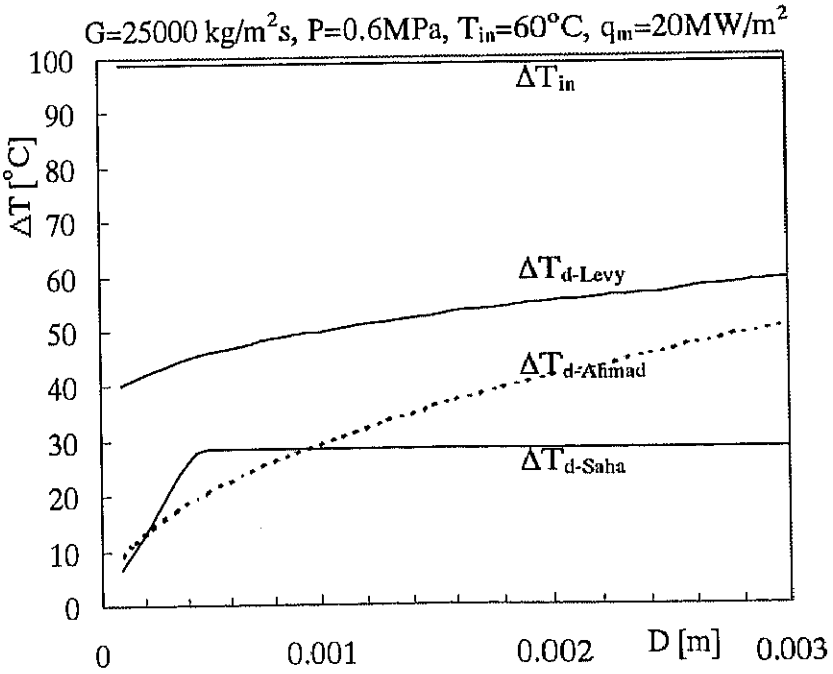

Fig. 6-4 Inner Diameter D Effect on the ΔT_d

6.1.1.1 4 The Inner diameter D Effect on the ΔT_d

Figure 6-4 shows the D effect on the ΔT_d. The Ahmad and the Levy models both show the increasing tendency with the increase of the diameter, while the Saha-Zuber model, with Pe number at 70000 as threshold, shows no relation with D at high Pe number and a steep increasing tendency at low Pe condition. The D effect shown from the Ahmad and the Levy models here is considered right. As we know, for single-phase liquid turbulent flow, with the increase of the D, heat transfer coefficient decreases and causes tube wall temperature increasing more quickly and making the bubble formation and detachment easily, that is, increase the ΔT_d value.

6.1.1.1 5 The Inlet Liquid Temperature Effect on the ΔT_d

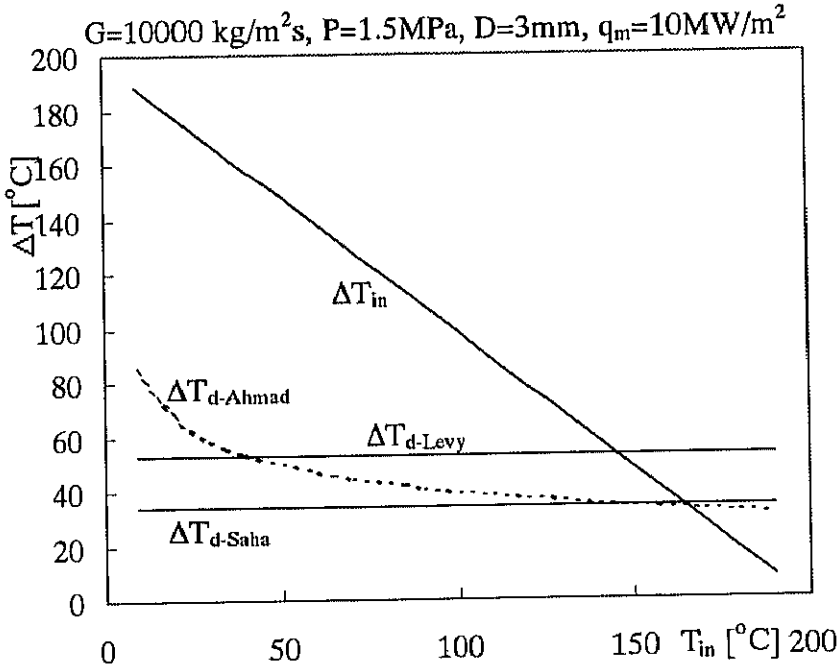

Fig. 6-5 Inlet Liquid Temperature Effect on the ΔT_d

In the above three models, only the Ahmad NVG model employs the inlet liquid temperature element. As shown in fig.6-5, with the change of the inlet temperature, the Levy and the Saha-Zuber model shows no change while the Ahmad model shows an obvious decreasing function, especially at low inlet temperature condition. When T_{in} is low enough, the Ahmad model is found obvious error. Analysis at G=4500 kg/m^{2}s, P=0.38 MPa, D=9.5 mm, L=0.6096 m and heat flux q_m=5 MW/m^2 are shown in Figs.6-6 and 6-7. Although ΔT_d is substituted by ΔT_{in} when the calculated ΔT_d is higher than ΔT_{in} (means the NVG begins at the tube inlet), the Ahmad model still shows giving a too high ΔT_d prediction at low inlet temperature condition (Fig.6-6). This directly affects χ_d and results χ_d in a too low value. The too low χ_d further makes an abnormal high χ_{out} (Fig.6-7) at low inlet temperature condition.

The abnormal is further enlarged when α_{out} is calculated and leads to an abnormal high α_{out} (Fig.6-7) and finally results a too low CHF prediction. Under above listed condition, when inlet temperature is 0.3°C, with using the Ahmad ΔT_d model, the predicted CHF is only 50% of the experimental CHF (Knoebel et al data, 1973). Therefore, under low inlet temperature condition, the Levy model is recommended.

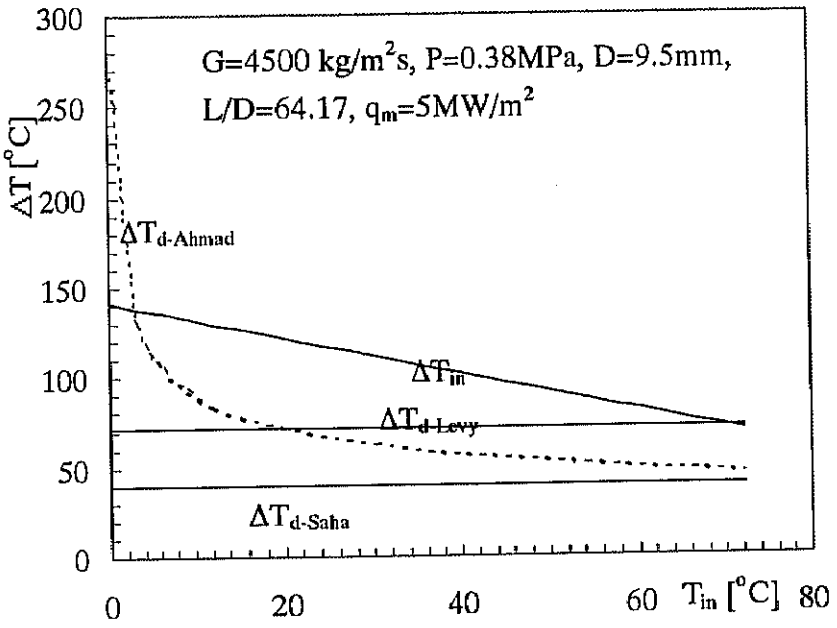

Fig. 6-6 Inlet Liquid Temperature T_{in} Effect on the ΔT_d, the Ahmad Model Gives Too High ΔT_d at Low Inlet Temperature

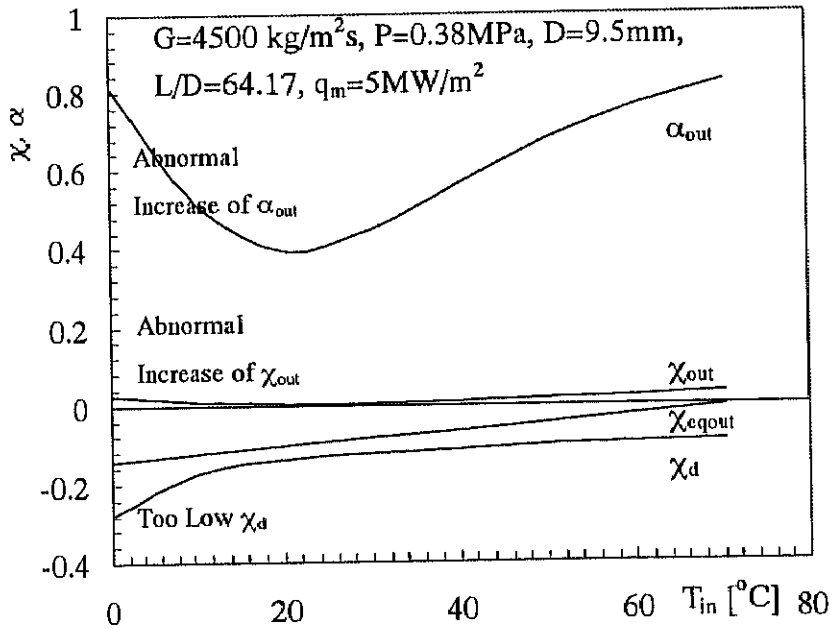

Fig. 6-7 Abnormal Increase of the True Quality and the Void Fraction at Low Inlet Temperature Due to the Predicted too High ΔT_d

6.1.1.1.6 The Heated Length Effect on the ΔT_d

No L element is employed in the ΔT_d calculation procedure, but this does not mean L does no effect on the CHF through affecting the ΔT_d. The decrease of the heated length requests a higher heat flux to ensure the NVG occurrence in the tube. This, actually, gives a reason for the L effect on the CHF, that is, the CHF increases with the decrease of L.

6.1.1.2 Model Recommendation for the NVG Prediction

A rough analysis to the reasonability of the above three NVG models can also be carried out with a so-called statistic way. As we know, in most situations, for the subcooled flow boiling, the first kind of flow pattern (fig.1-2) happens. Therefore, in most situations, the CHF happens in the afterward region of the NVG point, that is, the CHF happens with the premise that the NVG point has been established. So, with a big amount experimental CHF data reported in the appendix 1, we can give the above 3 NVG models a rough inspection. We found that the Saha-Zuber model gives too low ΔT_d prediction. It even often predicts no NVG occurrence under the experimental CHF value. In the whole 2482 CHF data points, with the Saha-Zuber models, 1268 points predict no NVG occurrence in the tube under the experimental CHF value. The failing percent is as high as 51.1%(Table 6-1). The too low ΔT_d prediction tendency is much more obvious at high pressure and high mass flux condition. When pressure is over than 15MPa, with the Saha-Zuber model, about 77.5% data fail in the NVG prediction. When mass velocity is over than 30000 kg/m^2s, the un-predicting percentage reaches 98.4%. As shown in table.6-1, although the Levy model and the Ahmad model also predict no NVG occurrence sometimes at the experimental CHF value, the percentage is low and is considered reasonable. (Besides the CHF mechanism (liquid sublayer dryout model) based on the occurrence of the first kind of flow pattern (fig.1-2), although seldom encountered, another kind of CHF triggering mechanism, that the CHF may happens before the NVG point, is considered existing for the happening of the second kind of flow pattern (fig.1-3)).

Table 6-1 NVG Failing Prediction Points and Percentage at the Experimental CHF Value

Model	Whole Points	Failing Prediction Points	Failing Percent
Saha	2482	1268	51.1%
Levy	2482	147	5.9%
Ahmad	2482	261	10.5%

Compared with the Saha-Zuber model, generally, the NVG prediction value from the Levy and the Ahmad models does not differ too much. It has been shown (figs. 6-6, 6-7) that at low inlet temperature condition, the Ahmad model is not good enough. Also, from the whole CHF prediction results, it's found that the Levy model shows better prediction at high mass velocity condition (generally accompanied by the low D condition). Therefore, a rough recommendation for the calculation of the NVG point is given as following:

a. The Levy and Ahmad models are much more preferred than the Saha-Zuber model.

b. Although either the Levy model or the Ahmad model can be used, generally the Ahmad model shows giving a better prediction than the Levy model.

b. The Levy NVG model is recommended at low inlet temperature (T_{in}<30°C).

c. The Levy NVG model is not recommended for low mass velocity condition (G<4000 kg/m^{2}s). But the model shows better prediction ability for high mass velocity condition (G ≥ 40000 kg/m^{2}s, which generally companied by small tube diameter).

Therefore, for water, an optimized method for the NVG prediction is developed by the combination of both the Levy and the Ahmad model. The method is depicted as:

a. Generally, $\Delta T_d=\Delta T_{d\text{-}Ahmad}$;

b. If T_{in}<30°C or G ≥ 40000 kg/m^{2}s, $\Delta T_d=\Delta T_{d\text{-}Levy}$

6.1.1.3 Sensitivity Study

The sensitivity studies compare the present model's prediction in this section using the Shah-Zuber, Levy, Ahmad models and the recommended optimized NVG method. The data used for sensitivity study are the data shown in the appendix 1, with subtracting the low L/D data (L/D <20).

Table 6-2 Comparisons of the Predictions from the NVG Correlations

Error Band / Model	±5 (%)	±10 (%)	±15 (%)	±20 (%)	±25 (%)	±30 (%)	±35 (%)	±40 (%)	±45 (%)	±50 (%)	R.M.S (%)
Saha	8.83	17.15	25.52	33.26	42.99	51.18	61.74	71.84	78.66	84.71	39.03
Levy	33.42	50.84	64.53	75.13	82.04	86.81	90.31	93.27	95.18	96.77	21.09
Ahmad	28.33	51.89	66.67	77.04	85.08	91.59	94.63	96.09	97.14	97.86	19.27
Optimized	35.83	59.66	74.62	85.22	90.36	94.04	95.95	96.95	97.54	97.86	17.42

6.1.2 The True Quality

6.1.2.1 Comparisons for the True Quality Models

For the calculation of real quality, here we only give comparisons to three typical calculation ways.

(1) Mechanistic Model (Jafri, Dougherty and Yang, 1995)

The model is developed from the mass energy balance with a form of differential equation:

$$\frac{dx}{dx_{eq}} = 1 + \frac{x - x_{eq}}{(1-x)x_d} \qquad (6\text{-}8)$$

with initial condition: when $\chi_{eq}=\chi_d$ (at NVG point), $\chi=0$

The true quality calculated from eq.6-8 is called χ_1 in this chapter.

(2) Profile-Fit Model

In the model, no attempt is made to describe the detailed local process, and an arbitrary interpolation formula is used to fit the quality profile from the NVG onward. The Levy famous profile-fit model is written as eq.6-9. Eq.6-10 was proposed by Ahmad (1971) and Saha-Zuber (1974) separately. Although written in different form, the basics of Kroger-Zuber (1969) model are the same as what is in the Ahmad and the Saha-Zuber model as eq.6-10. Eq.6-9 is considered only an approximation of eq.6-10.

$$x = x_{eq} - x_d e^{(x_{eq}/x_d - 1)} \qquad (6\text{-}9)$$

$$x = \frac{x_{eq} - x_d e^{(x_{eq}/x_d - 1)}}{1 - x_d e^{(x_{eq}/x_d - 1)}} \qquad (6\text{-}10)$$

From the deriving procedure, the profile-fit model is found only a good approximation of the Jafri model.

The true quality calculated from eq.6-10 is called χ_2 in this chapter.

(3) Mechanistic Model with Considering Condensation Effect

In the model, an attempt was made to describe the process of bubble formation and condensation. Detailed survey of the method was given by Lahey & Moody (1977). Although the model is capable of qualitative description of the phenomena, it contains, of necessity, a number of empirical functions describing the rates of the various processes. As recommended by Lahey & Moody (1977), the true quality χ is calculated iteratively from the following procedure.

a. Assume a χ

$$H_l = \frac{H_{lin} + 4 \times q_m \times L/(G \times D) - H_g x}{1 - x} \quad (6\text{-}11)$$

b. From the χ, calculate void fraction α, Lahey & Moody (1977) recommended the Dix model (1971):

$$\alpha = \frac{x}{C_0\left[x + \frac{\rho_g}{\rho_f}(1-x)\right] + \frac{\rho_g V_{gj}}{G}} \quad (6\text{-}12)$$

where $C_0 = \gamma\left[1 + \left(\frac{1}{\gamma} - 1\right)^b\right]$, $\gamma = \frac{x}{x + \frac{\rho_g}{\rho_f}(1-x)}$, $b = \left(\frac{\rho_g}{\rho_f}\right)^{0.1}$

$$V_{gj} = 2.9\left[\frac{(\rho_f - \rho_g)\sigma g}{\rho_f^2}\right]^{1/4}$$

c. Calculate χ

$$\begin{cases} \text{For } H_l \geq H_{ld},\ q_{cond} = 0.075 \dfrac{H_{fg} D \alpha}{4\left(\frac{1}{\rho_g} - \frac{1}{\rho_f}\right)}(T_{SAT} - T_l) \\ \text{For } H_l \leq H_{ld},\ q_{cond} = 0 \end{cases} \quad (6\text{-}13)$$

$$\begin{cases} \text{For } H_l \geq H_{ld},\ q_b = q\dfrac{h_l - h_{ld}}{h_f - h_{ld}} \\ \text{For } H_l \leq H_{ld},\ q_b = 0 \end{cases} \quad (6\text{-}14)$$

$$x = \frac{4(L - Z_0)}{GDH_{fg}}\left(\frac{q_b}{1+\varepsilon} - q_{cond}\right) \quad (6\text{-}15)$$

with $\varepsilon = \dfrac{\rho_f(H_f - H_l)}{\rho_g H_{fg}}$

The models also employs the initial condition that: χ=0 at NVG point ($\chi_{eq}=\chi_d$).

The true quality calculated from above procedure is called χ_3 in this chapter.

In the following, the three models are compared at different pressure and mass velocity conditions. The mass flux G effect is shown in Fig.6-8. The true quality decreases significantly with the increase of the mass velocity G. The models 1 and 2 seem giving almost same predictions at low-pressure condition while the model 3 gives a much lower χ

prediction. P effect is shown in fig.6-9. The true quality shows a decrease function of the pressure P. Although the models 1 and 2 give almost same prediction at low pressure (P=0.1MPa), their difference appears when the pressure increases. The model 2 gives a little lower quality prediction at high pressure than the model 1, which in turn, would result a too high CHF prediction. This is considered a reason for the high CHF tendency at low L/D condition that happens easily under high-pressure condition.

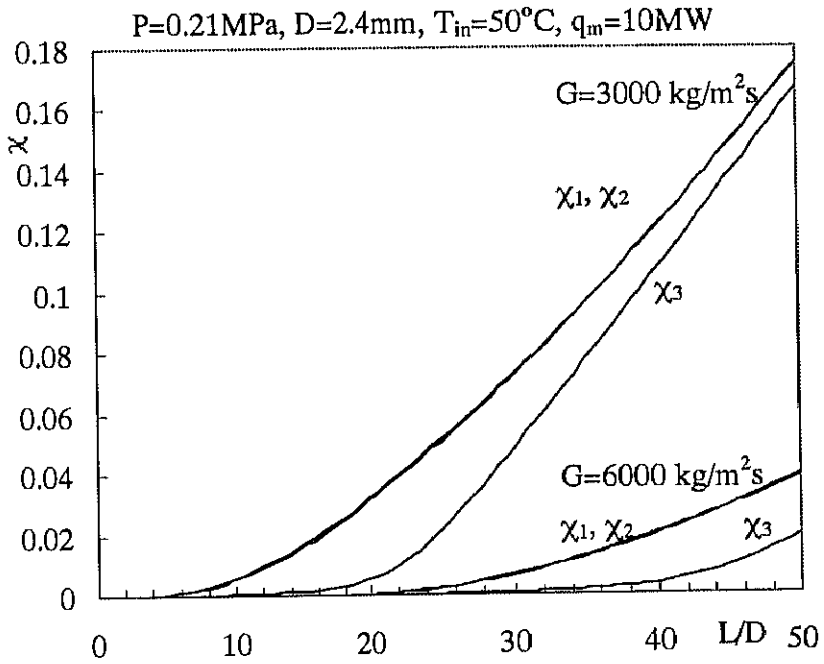

Fig.6-8 True Quality Distribution along the Tube at Different Mass Flux

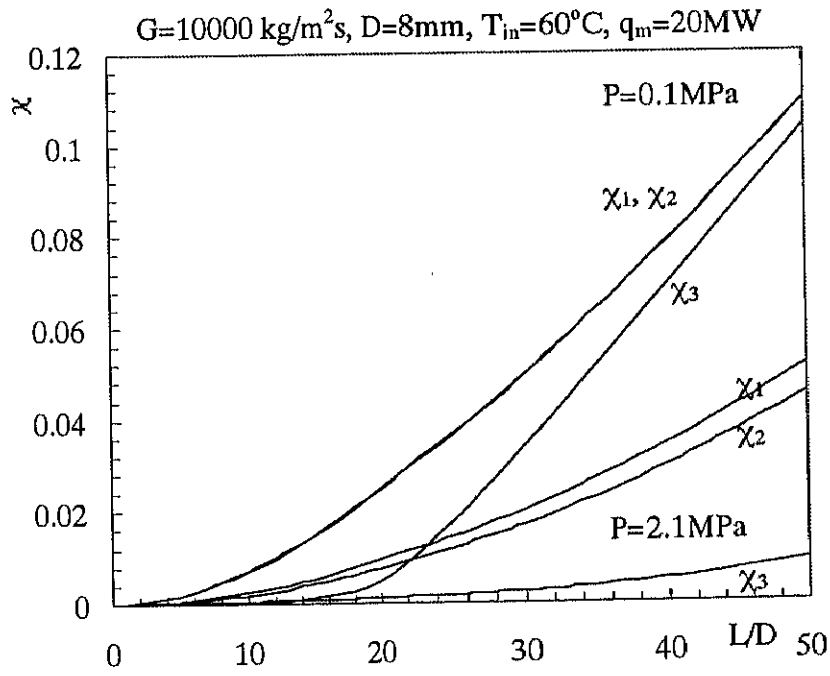

Fig.6-9 True Quality Distribution along the tube at Different Pressure

Besides the above discussed G and P effect, the inner diameter affect χ through its effect on the NVG point. The increase of D increases the true quality χ. The ratio of the heated length to the inner diameter L/D affects χ through its effect on the exit equilibrium quality. The χ increases with the increase of L/D.

6.1.2.2 Model Recommendations for the True Quality Calculation

As analyzed above, although the model 3, the mechanistic model with considering condensation effect, is capable of qualitative description of the phenomena, it contains a number of empirical functions describing the rates of the various processes. There is no completely general such a mechanistic model. The model is therefore considered to be too empirical. The comparisons in figs. 6-8 and 6-9 also show that the model has too low true quality prediction tendency. Therefore, the model is firstly put aside with no more consideration.

From the model deriving procedure, the Jafri model, which developed only on the base of the heat and mass balance, is most recommended. The profile-fit model that developed by Ahmad, Saha-Zuber and Levy et al is a good approximation of the Jafri model. Besides, because the advantages of easily using and well accepted, the profile-fit model is adopted in the present CHF prediction procedure. But as mentioned above, for the approximation characteristics, the using of the profile-fit model is analyzed a reason for the over-prediction tendency at low L/D, which happens easily under high-pressure condition.

6.1.2.3 Sensitivity Studies

The sensitivity studies compare the present model's prediction in this section using the mechanistic model by Jafri, profile-fit model by Ahmad and mechanistic model with considering condensation effects recommended by Lahey. The data used for sensitivity study are the data shown in appendix 1, with subtracting the low L/D data (L/D <20).

Table 6-3 Comparisons of the Predictions from the True Quality Correlations

Error Band / Model	±5 (%)	±10 (%)	±15 (%)	±20 (%)	±25 (%)	±30 (%)	±35 (%)	±40 (%)	±45 (%)	±50 (%)	R.M.S (%)
1(Jafri)	35.52	59.35	74.4	84.36	91.41	94.63	96.18	97.23	97.64	97.91	16.93
2(Ahmad et al)	35.83	59.66	74.62	85.22	90.36	94.04	95.95	96.95	97.54	97.86	17.42
3(Lahey & Moody)	9.95	18.98	25.46	30.61	36.82	42.2	47.08	51.41	55.7	64.37	58.85

6.1.3 The Void Fraction

6.1.3.1 Comparisons for the Void Fraction Models

There are also three main ways to calculate void fraction. From basic principles and definitions of the two-phase flow, void fraction can be written as only a function of the true quality χ and slip ratio S as:

$$\alpha = \frac{\chi}{\chi + \left(\frac{\rho_g}{\rho_f}\right) S(1-\chi)} \qquad (6\text{-}16)$$

(1) Ahmad model (1970)

Ahmad model calculates the slip ration S from:

$$S = \left(\frac{\rho_f}{\rho_g}\right)^{0.205} \left(\frac{GD}{\mu_f}\right)^{-0.016} \qquad (6\text{-}17)$$

where the Ahmad void fraction model implies a vapor concentration parameter C_0 as:

$$C_0 = \frac{\frac{S - \rho_f V_{gj}}{G(1-\chi)} \rho_g (1-\chi) + \chi \rho_f}{\rho_g (1-\chi) + \chi \rho_f} \qquad (6\text{-}18)$$

(2) Kroger –Zuber (1968)

Zuber-Findlay (1965) recommended the void fraction calculated from:

$$\alpha = \frac{x}{C_0 \left[x + \frac{\rho_g}{\rho_f}(1-x) \right] + \frac{\rho_g V_{gj}}{G}} \qquad (6\text{-}19)$$

where C_0 is vapor concentration parameter, V_{gj} is drift velocity. Eq.6-19 indicates the implicit S as:

$$S = C_0 + \frac{x(C_0 - 1)\rho_f}{\rho_g (1-x)} + \frac{\rho_f V_{gj}}{G(1-x)} \qquad (6\text{-}20)$$

Kroger-Zuber (1968) suggested C_0=1.13 and calculated Vgj from:

$$V_{gj} = 1.41 \left(\frac{\sigma g (\rho_f - \rho_g)}{\rho_f^2} \right)^{1/4} \qquad (6\text{-}21)$$

(3) Dix Model (1971)

Dix model employed the same void fraction expression as what used by Zuber-Findlay (eq.6-19). But the C_0 is calculated from:

$$C_0 = \gamma\left[1+\left(\frac{1}{\gamma}-1\right)^b\right], \qquad (6\text{-}22) \quad \text{with} \quad \gamma = \frac{x}{x+\frac{\rho_g}{\rho_f}(1-x)}, \quad b = \left(\frac{\rho_g}{\rho_f}\right)^{0.1}$$

V_{gj} is calculated from: $$V_{gj} = 2.9\left[\frac{(\rho_f - \rho_g)\sigma g}{\rho_f^2}\right]^{1/4} \qquad (6\text{-}23)$$

The above three models show void fraction is only an obvious function of the true quality, pressure P and mass flux G. Fig.6-10 shows the void fraction versus quality with the change of pressure. The void fraction decreases with the increase of pressure. The three models show giving generally same void fraction results at high quality region. Significant difference lies only in the low quality region, that is, the region near the NVG point. In this low quality region, the Ahmad and Kroger-Zuber model predict the same tendency while the Dix model gives a higher prediction.

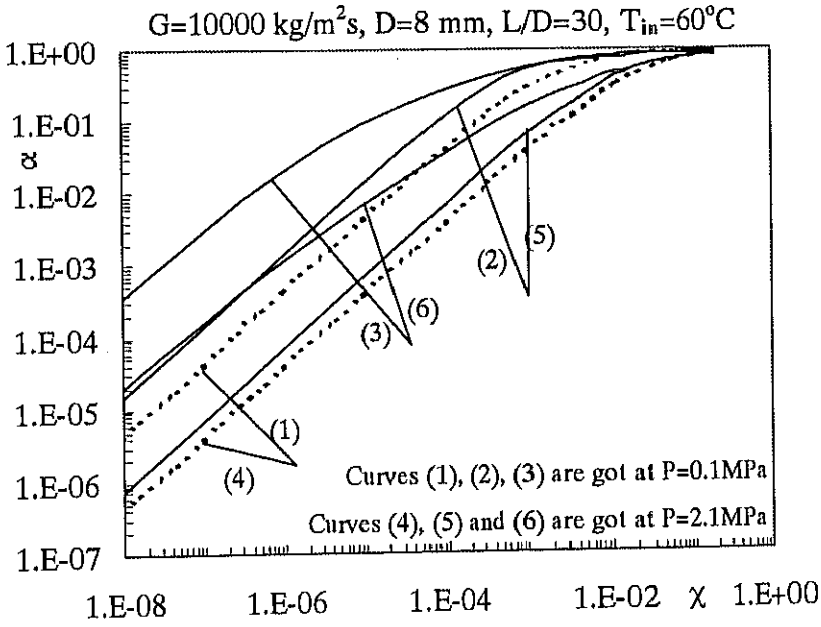

(1), (4) Ahmad Model; (2), (5) Kroger-Zuber Model; (3), (6) Dix Model

Fig. 6-10 Comparisons for the Three Void Fraction Models

From the physical meaning of the vapor concentration parameter C_0, as shown in fig.6-11 (Lahey and Moody, 1977, P203), C_0 changes with the change of the boiling region. At low quality region, the boiling mode falls in the initial or middle stage of developing bubbly flow, the corresponding concentration parameter C_0 then should be lower than 1. At the working condition in the fig.6-10, the C_0 comparisons among the three models are shown

in fig.6-12. We found that in the low quality condition, the Ahmad model gives too high C_0 (up to 4); the Kroger-Zuber model keeps the C_0 at 1.13 and only the Dix model shows giving the reasonable C_0 value (C_0<1). Therefore, the Dix model is thought to be most reasonable at low quality region. At high quality region, where the flow pattern falls in the fully developed bubbly flow (or slug flow) region, the Ahmad and Kroger-Zuber models show the appropriate C_0 and therefore be suitable for the void fraction prediction. Generally, because the point need calculating always falls in this non- low-quality region, the Ahmad and Kroger-Zuber model are therefore found meeting the general requirements. But for the low quality region, for example, such as the point near the NVG point, the Dix model is more reasonable.

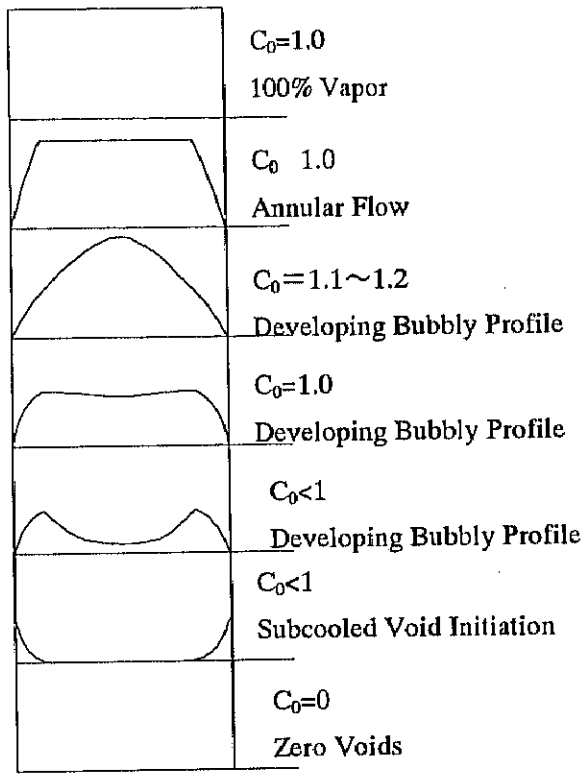

Fig.6-11 Corresponding Relations Between the Flow Regimes and Diabetic Void Concentration Profiles

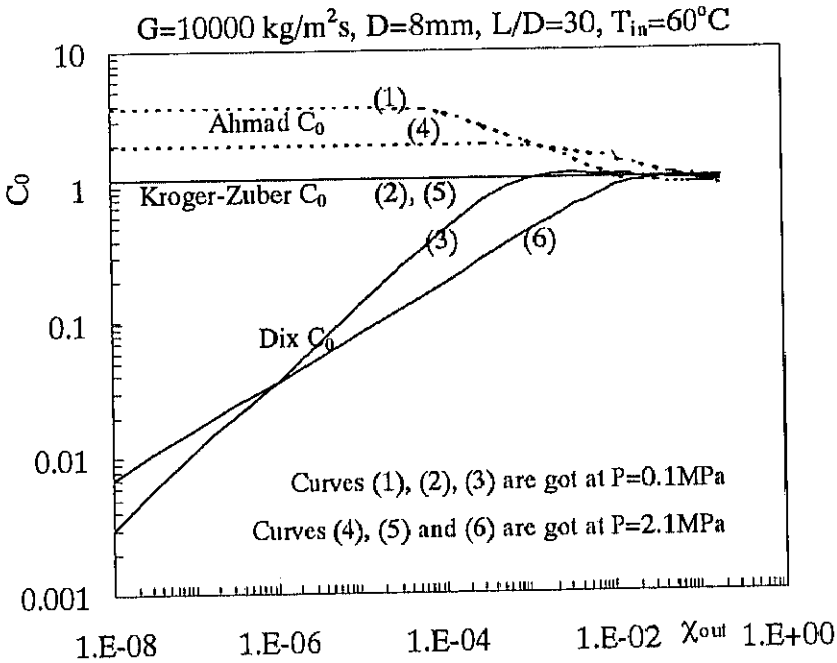

(1), (4) Ahmad model; (2), (5) Kroger-Zuber model; (3), (6) Dix model

Fig. 6-12 Comparisons for the Vapor Concentration Parameter C_0 in the Three Models

6.1.3.2 Recommendation for the Void Fraction Calculation

Any of the above three introduced model can be used for the prediction of the void fraction. Although differing not too much in the non-low quality region, the Ahmad and Kroger-Zuber models are found a general better prediction than the Dix model. But from the analysis to vapor concentration parameter at low quality region, the Dix model is most reasonable for the low quality region. In the proposed CHF model, the Ahmad model is finally adopted for the general rightness and simplicity. But the using of the Ahmad void fraction model is considered one of the reasons for the over-prediction tendency at low L/D condition. At low L/D condition, where the exit is much near the NVG point, the adoption of the Dix model can moderate the CHF over-prediction a lot.

6.1.3.2 Sensitivity Studies

The sensitivity studies compare the present model's prediction in this section using the Ahmad, Kroger-Zuber and Dix void fraction models. The data used for sensitivity study are the data shown in the appendix 1, with subtracting the low L/D data (L/D <20).

Table 6-4 Comparisons of the Predictions from the Void Fraction Correlations

Error Band / Model	±5 (%)	±10 (%)	±15 (%)	±20 (%)	±25 (%)	±30 (%)	±35 (%)	±40 (%)	±45 (%)	±50 (%)	R.M.S (%)
Ahmad	35.83	59.66	74.62	85.22	90.36	94.04	95.95	96.95	97.54	97.86	17.42%
Kroger-Zuber	28.65	55.53	71.99	81.9	90.36	93.95	96.41	97.32	97.86	98.36	16.67%
Dix	24.1	48.89	69.17	82.49	90.68	94.72	96.73	98.23	99	99.36	15.49%

6.1.4 The Bubble Drag Coefficient

Drag coefficient is involved in the computation process of the sublayer thickness. In literature, Harmathy (1960) and Chan & Prince (1965) correlations are for selection.

Harmathy: $$C_D = \frac{2}{3}\frac{D_B}{\left(\frac{\sigma}{g(\rho_f - \rho_g)}\right)^{0.5}} \qquad (6\text{-}24)$$

Chan & Prince $$C_D = \frac{48\mu_f}{\rho_f D_B (U_B - U_{BL})} \qquad (6\text{-}25)$$

where (U_B U_{BL}) is the relative velocity of the bubble with respect to the liquid at the position corresponding to the centerline of the vapor blanket.

Both the Harmathy and Chan & Prince models are found can be used for the CHF prediction in the present model. Generally, The using of the Harmathy model shows a higher CHF prediction tendency than the using of the Chan-Prince model. Better CHF agreement is got with the employing the Chan-Prince drag coefficient. The Harmathy correlation, which is derived from the buoyancy and surface tension forces balance, is recommended in the present CHF model at low pressure (P<1MPa). The latter one proposed for small bubble that is dominated by viscous forces is recommended at medium and high pressure (P ≥ 1MPa).

The sensitivity studies compare the present model's prediction in this section using the Harmathy and Chan & Prince correlations and the recommended optimized drag coefficient method. The data used for sensitivity study are the data shown in the appendix 1, with subtracting the low L/D data (L/D <20).

Table 6-5 Comparisons of the Predictions from the Drag Coefficient Correlations

Error Band / Model	±5 (%)	±10 (%)	±15 (%)	±20 (%)	±25 (%)	±30 (%)	±35 (%)	±40 (%)	±45 (%)	±50 (%)	R.M.S (%)
Harmathy	34.33	56.21	72.44	83.17	88.31	91.81	93.86	95.23	96.13	96.82	20.44
Chan	33.74	58.94	73.44	82.9	89.86	93.59	95.95	96.95	97.59	98.04	17.69
Optimized	35.83	59.66	74.62	85.22	90.36	94.04	95.95	96.95	97.54	97.86	17.42

6.2 DISCUSSION OF THE HELMHOLTZ INSTABILITY WAVELENGTH IN FINITE SYSTEM

As we know, originally, for an instability wave existing at the interface of liquid phase and gas phase (fig.6-13), the Helmholtz instability wavelength is written as:

$$\lambda = \frac{2\pi\sigma}{(U_g - U_l)^2}\left(\frac{1}{\rho_g I_g} + \frac{1}{\rho_l I_l}\right) \qquad (6\text{-}26)$$

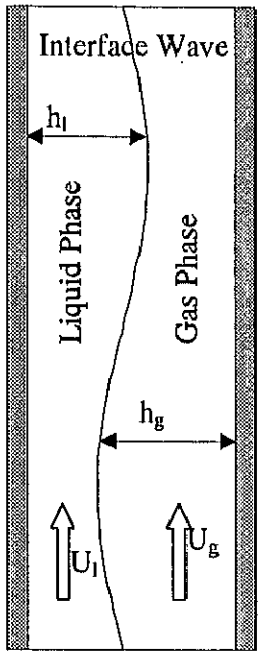

Fig. 6-13 Configuration of Instability Wave
at the Interface of Liquid and Gas Phases

where U_g and U_l are average velocities of the liquid and the gas phase respectively. λ is wavelength. I_l and I_g are defined as:

$$I_l = \coth(2\pi\frac{h_l}{\lambda}) \qquad (6\text{-}26a)$$

$$I_g = \coth\left(2\pi\frac{h_g}{\lambda}\right) \qquad (6\text{-}26b)$$

where h_l and h_g are average heights of the liquid and gas phase respectively. For the mathematics characteristics of coth function, I_l and I_g can be simplified as:

When $h_l/\lambda, h_g/\lambda < 0.1$, $I_{l(g)} = \coth\left(\frac{2\pi h_{l(g)}}{\lambda}\right) \approx \frac{\lambda}{2\pi h_{l(g)}}$

Further when h_l/λ and h_g/λ are small enough, I_l and I_g will be very big, which make the $1/I_{l(g)}$ can be taken as zero.

When $\frac{h_l}{\lambda}, \frac{h_g}{\lambda} > 0.25$, $I_{l(g)} = \coth\left(\frac{2\pi h_{l(g)}}{\lambda}\right) \approx 1$

Applying the above critical wavelength to subcooled vertical flow boiling situation, as shown in fig.6-14, with the assumption that $L_B = \lambda_1 = \lambda_2$, the critical wavelengths at interfaces I and II are written as:

$$L_B = \lambda_1 = \frac{2\pi\sigma}{U_B^2}\left(\frac{1}{\rho_l I_{l1}} + \frac{1}{\rho_g I_g}\right) \qquad (6\text{-}27)$$

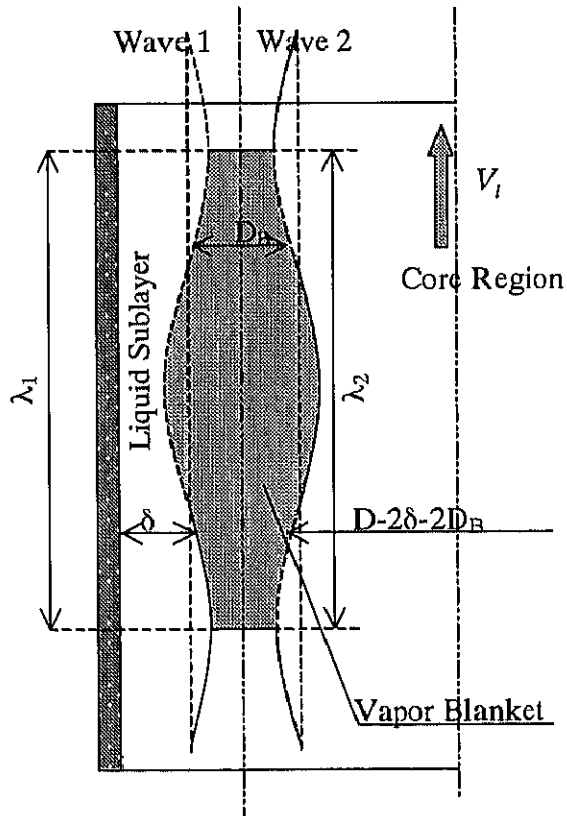

Fig. 6-14 Configuration of the Instability Waves at the Two Liquid-Vapor Interfaces

$$L_B = \lambda_2 = \frac{2\pi\sigma}{(V_c - U_B)^2}\left(\frac{1}{\rho_g I_g} + \frac{1}{\rho_c I_{l2}}\right) \qquad (6\text{-}28)$$

where $I_{l1} = \coth\left(\frac{2\pi\delta}{L_B}\right)$, $I_g = \coth\left(\frac{2\pi D_B}{L_B}\right)$;

$$I_{l2} = \coth\left(\frac{2\pi(D - 2\delta - 2D_B)}{L_B}\right)$$

Researches are carried out to get a whole impression to the values of the δ/L_B, D_B/L_B, $(D-2\delta-2D_B)/L_B$ and I_{l1}, I_g, I_{l2} at the CHF condition. The researches cover a wide range of operating conditions (2482 points shown in appendix 1). The results are shown in tables 6-6 and 6-7 respectively.

Table 6-6 Impressions of the δ/L_B, D_B/L_B and $(D-2\delta-2D_B)/L_B$ Values

δ/L_B	D_B/L_B	$(D-2\delta-2D_B)/L_B$
0.00024—0.00974	0.0086—0.343	0.529—658
90.8% falls in the scope: 0.0024—0.003	98.03% data < 0.25 77.33% data < 0.1	100% data >0.25

Table 6-7 Impressions of the I_{l1}, I_g and I_{l2} Values

I_{l1}	I_g	I_{l2}
670.5—16.4	18.6—1.02	1.003—1
90.8% data fall in scope: 663.15—53.1	25.9%, $0.5<I_g<2$ 49.3%, $2<I_g<5$ 12.8%, $5<I_g<8$ 3.72%, $8<I_g<10$ 8.35%, $10<I_g<18.6$	100% fall in scope: 1.003—1

With the tables 6-6 and 6-7, we get that for the most of δ/L_B is very small, I_{l1} turns to be very high. This makes $1/(\rho_l I_{l1})$ item in the eq.6-27 can be taken as 0. And because the most of $(D-2\delta-2D_B)/L_B$ value are big enough, It's also reasonable to simplify the I_{l2} to 1 in the eq.6-28.

Question lies in the simplification of I_g. As shown in the above tables, the D_B/L_B seems to be not so big and not so small. For about 93% of D_B/L_B data is lower than 0.25, it's difficult just to simplify I_g to 1 although it has been taken as granted in every liquid sublayer CHF model (Lee-Mudarwar, Katto, Celata and present model). It's also

unreasonable to neglect the $1/I_g$ item. But as what have been mentioned, when $\frac{h_{l(g)}}{\lambda} < 0.1$, $I_{l(g)} = \coth\left(\frac{2\pi h_{l(g)}}{\lambda}\right) \approx \frac{\lambda}{2\pi h_{l(g)}}$. This seems more suitable for the I_g. Therefore, it is more reasonable to write I_g as:

$$I_g = \coth\left(\frac{2\pi D_B}{L_B}\right) \approx \frac{L_B}{2\pi D_B}$$

Then, eqs.6-27 and 6-28 turn to:

$$L_B = \lambda_1 = \frac{2\pi\sigma}{U_B^2}\frac{2\pi D_B}{\rho_g L_B} \qquad (6\text{-}29)$$

$$L_B = \lambda_2 = \frac{2\pi\sigma}{(V_c - U_B)^2}\left(\frac{2\pi D_B}{\rho_g L_B} + \frac{1}{\rho_c}\right) \qquad (6\text{-}30)$$

With the assumption $L_B = \lambda_1 = \lambda_2$, U_B is written as:

$$U_B = \frac{V_c^2}{\frac{\sigma}{\rho_c\sqrt{\frac{\sigma D_B}{\rho_g}}} + 2V_c} \qquad (6\text{-}31)$$

As having been pointed, present CHF model gives too high prediction at low L/D condition (especially at L/D < 5). Although not significant, the using of eq.6-31 instead of eq.3-3 in the calculation procedure do decrease the predicted CHF at low L/D condition someway, showing a better coincidence with experimental data.

As shown in table 6-8, the sensitivity studies compare the present model's prediction in this section using the eq.3-3 and eq.6-31 for the U_B calculation. The data used for sensitivity study are the data shown in appendix 1, with subtracting the low L/D data (L/D <20). Although a little different in appearance, because both the equations (eq.6-31 and eq.3-3) can be approximately written in $U_B \approx V_c/2$, the using of the either of the two equations therefore gives no big difference in the CHF prediction result.

Table 6-8 Comparisons of the Predictions from the Different U_B

Error Band / U_B from	±5 (%)	±10 (%)	±15 (%)	±20 (%)	±25 (%)	±30 (%)	±35 (%)	±40 (%)	±45 (%)	±50 (%)	R.M.S (%)
Eq.3-3	35.83	59.66	74.62	85.22	90.36	94.04	95.95	96.95	97.54	97.86	17.42
Eq.6-31	35.79	59.57	73.12	81.99	89.31	93.63	95.91	97.14	97.68	98	17.61

6.3 CHF UNDER EXTREME CONDITION

As reported in the chapter 4, the proposed liquid sublayer dryout mechanism shows an over prediction tendency at low L/D value, especially at high-pressure condition. Besides the errors in the Ahmad true quality and void fraction model analyzed in the Chapters 6.1.2 and 6.1.3, another reason for the over-prediction is considered due to the change of the CHF triggering mechanism.

Also, as reported in the chapter 4, under some extreme condition, such as at high pressure ($P \geq 17.5$ MPa) or high mass flux ($G \geq 50000$ kg/m^{2}s, with the CHF up to 100 MW/m^2), with the proposed liquid sublayer dryout model, sometimes the final calculated q doesn't equal to the assumed q_m even when the assumed q_m has converged to a point. Although the CHF under such circumstance is finally calculated successfully by doing modification to the Levy D_B (by increasing D_B step by step) with the calculated CHF actually the lowest possible CHF value q_{NVG}, the true reason for the unpredictable is considered due to the change of the CHF triggering mechanism.

Following gives a brief discussion for the changed CHF triggering mechanism.

6.3.1 Corresponding Relations between the Flow Patterns and the CHF Triggering Mechanisms

The subcooled flow boiling CHF triggering mechanism is considered tightly connected to the flow pattern. Two kinds of flow pattern are reported in literature. The first one, as shown in fig.1-2, which is well encountered, includes the single-phase flow, bubbly flow and the slug flow regions. While the second kind of pattern, as shown in fig 1-3, includes the nucleate boiling flow and inverted annular flow regions and is characterized by the appearance of explosive-like film boiling at some point in the nucleate boiling region. The second kind of flow pattern is seldom encountered and happens easily only under extremely high pressure or extremely high mass flux condition.

Corresponding to the two kinds of flow pattern, two kinds of CHF triggering mechanism are considered existing at the same time with working in different scopes. The famous liquid sublayer dryout mechanism, which implies that the CHF happens in the afterward region of the NVG point, is considered working only for the first kind of flow pattern. The possible minimum CHF for the liquid sublayer dryout mechanism is restricted by q_{NVG}, the heat flux needed for the establishment of the NVG point at the tube exit (also the minimum heat flux needed for the establishment of the first kind of flow pattern). The highest possible CHF is restricted by q_{SAT}, the heat flux needed for heating all the subcooled liquid to the saturation condition. Therefore, the possible CHF for the liquid sublayer dryout mechanism is then in the scope:

$$q_{NVG} \leq CHF \leq q_{SAT}.$$

where the q_{NVG} and q_{SAT} are only determined by the working conditions (G, P, D, L/D and T_{in}) and are characteristic parameters of the subcooled flow boiling.

Besides the liquid sublayer dryout mechanism, the happening of the second kind of flow pattern, which is characterized by the occurrence of the film boiling, is considered another CHF triggering mechanism. The main reason for the over-prediction or the unpredictable points reported in the chapter 4 is considered due to this changed CHF triggering mechanism.

In the following, a criterion is developed to determine that, for a certain working condition, what kind of flow pattern will happen near the CHF.

6.3.2 Criterion For the Determination of the Flow Pattern near the CHF

6.3.2.1 The Criterion for the Determination of the Flow Pattern

As mentioned in the above, the characteristic of the second kind of flow pattern is the occurrence of the film boiling at some point in the nucleate boiling region. In literature, "foam limit" is one of the most popular assumptions for the interpretation of the happening of the film boiling (Spiegler et al, 1963). It assumes that if coolant is exposed to a wall whose temperature is higher than homogeneous nucleation temperature (also called "limiting liquid superheat" or "ultraheat"), vapor generates rapidly due to the homogeneous nucleation, with a result that vapor bubbles accumulation in high density at the interface between the wall and coolant. Generally, the homogeneous nucleation temperature is calculated from Lienhard (1976) correlation as:

$$T_{HN} = T_{SAT} + T_{cr} * \left(0.905 - \frac{T_{SAT}}{T_{cr}} + 0.095 \left(\frac{T_{SAT}}{T_{cr}} \right)^8 \right) \qquad (6\text{-}32)$$

where T_{cr} is thermodynamic critical temperature. The homogeneous nucleation temperature is only a function of pressure.

If we borrow the "foam limit" theory as the reason for the occurrence of the film boiling in the second kind of flow pattern, the determining condition for the development of the flow pattern is the wall temperature distribution along the tube. If the tube wall temperature exceeds the homogeneous nucleation at some point (region), the second kind of flow pattern happens. Otherwise the flow pattern may develop as the first kind of flow pattern.

The wall temperature variation along the tube for the first kind of flow pattern is shown in fig.1-4. In the single-phase region, the wall temperature rises linearly. With the onset of nucleate boiling (point B), the wall temperature begins to level off, as more nucleation sites are activated beyond the ONB. The region BC is the partial boiling region and the region after point C is the fully developed boiling region, or FDB. The highest wall temperature is reached at point C and in the downward region of the point C the tube wall temperature keeps almost constant. Researches show that the heat flux/surface temperature relationship in the

fully developed region is, to a first approximation, independent of mass velocity and subcooling. Among lots of works reported in literature, The Thom correlation (1965), which was recommended by Collier (1981), Rohsenow (1985) and Celata (1997), is adopted in the current paper for the calculation of the highest wall temperature. The Thom correlation is written as eq.6-33.

$$T_w = T_{SAT} + 22.65 \times \left(\frac{q}{1000000}\right)^{0.5} \times e^{(-P/8.7)} \qquad (6\text{-}33)$$

For a certain subcooled flow boiling condition, the flow pattern near the CHF can be firstly judged by comparing the highest wall temperature with the homogeneous nucleation temperature. As mentioned above, q_{NVG} is the lowest heat flux needed for the establishment of the first kind of flow pattern. If at this lowest heat flux, the wall temperature in the fully developed region (highest wall temperature in the tube) is even higher (equal) than (to) the homogeneous nucleation temperature, the explosive-like film boiling will happen before the NVG point is established. Under such circumstance, the second kind of flow pattern happens and the first kind of flow pattern cannot be established at all. Therefore the flow pattern near the CHF can be determined through the following procedures:

(1) Under a certain condition, calculate the q_{NVG}.

(2) Under the working pressure, calculate the homogeneous nucleation temperature T_{HN} from eq.6-32.

(3) Calculate the wall temperature in fully developed region T_w at q_{NVG} from eq.6-33.

(4) Compare the T_w with T_{HN}:

(a) If $T_w < T_{HN}$, no film boiling occurs at q_{NVG}. The first kind of flow pattern can be established. Under such circumstance, the CHF may be triggered by the liquid sublayer dryout mechanism. The data is called in this paper as the first kind of data group.

(b) Else, if $T_w \geq T_{HN}$, explosive-like film boiling occurs before or at q_{NVG}. The second kind of flow pattern happens and the first kind of flow pattern can not be established. The explosive-like film boiling is assumed triggering the CHF. The data is called in this paper as the second kind of data group.

The changes of the highest wall temperature in the subcooled flow boiling and the homogeneous nucleation temperature with the change of pressure are shown in fig.6-15. Both of the temperatures increase with the increase of the pressure, but the wall temperature increases much quicker than the homogeneous nucleation temperature when the pressure is not too high ($P \leq 5$ MPa).

With combining the Lienhard T_{HN} and Thom T_w, under a certain pressure, there exists a critical value of q_{NVG}. If a working condition possesses a lower q_{NVG} than the corresponding critical q_{NVG} at the same pressure, the first kind of flow pattern can be established. While if a

working condition possesses a higher q_{NVG} than the corresponding critical q_{NVG}, the film boiling occurs before the NVG point is established and the first kind of flow pattern cannot be established at all. The critical q_{NVG} is calculated when the highest wall temperature just reaches the homogeneous nucleation temperature. The relation between the critical q_{NVG} and pressure P is shown in fig.6-16. The critical q_{NVG} decreases significantly with the increase of the pressure.

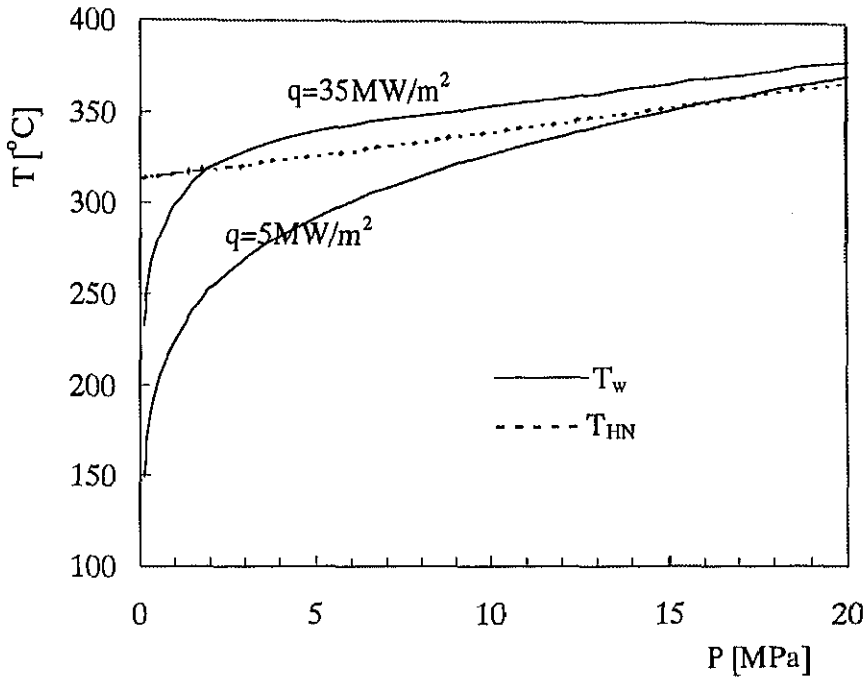

Fig.6-15 Configuration of the Changes of the T_w and the T_{HN} with the Change of Pressure

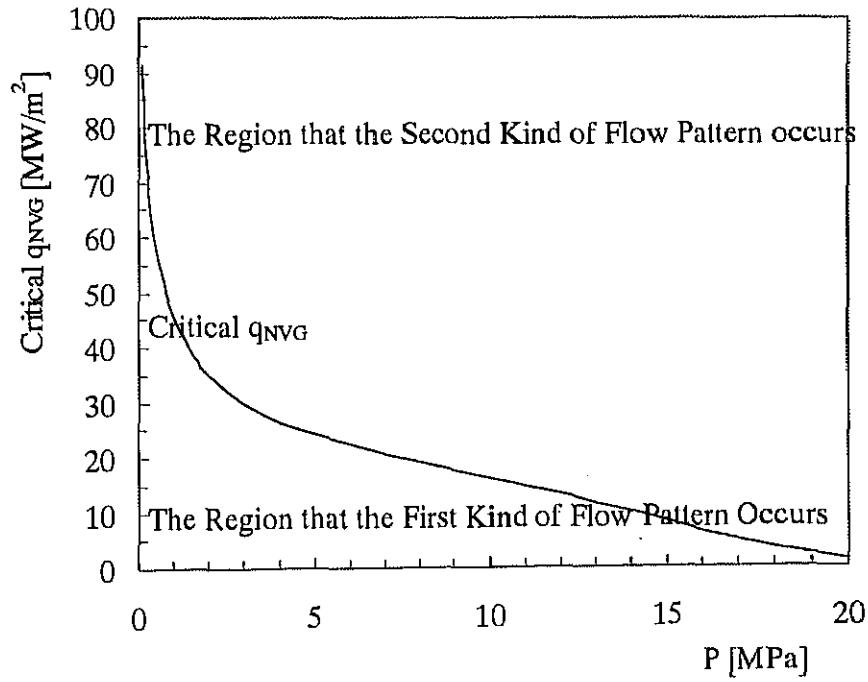

Fig.6-16 Critical q_{NVG} versus Pressure

From the definitions of the q_{NVG} and the critical q_{NVG}, any way that may result the increase of the q_{NVG} (such as increase G, decrease D or L/D) or the decrease of the critical q_{NVG} (such as increase P) can make the second kind of flow pattern much easily happen. Therefore, the second kind of data is generally characterized by extremely high CHF value (accompanied by high mass flux, low diameter or low L/D) or extremely high pressure.

6.3.2.2 Data Categorizing

With the big database (Appendix 1), a first step of data categorizing is carried out according to whether the first kind of flow pattern can be established or not. The result is shown in fig.6-17. In the total 2482 data points, with the Levy (Ahmad) NVG model, predominant 2151 (2190) data possess a lower q_{NVG} than the critical q_{NVG} and fall in the region lower than the curve, while 331 (292) points are predicted with a higher q_{NVG} and fall in the region above the critical q_{NVG} curve. All the unpredictable points (143 points) reported in the chapter 4.1 are found falling in the second kind of data group.

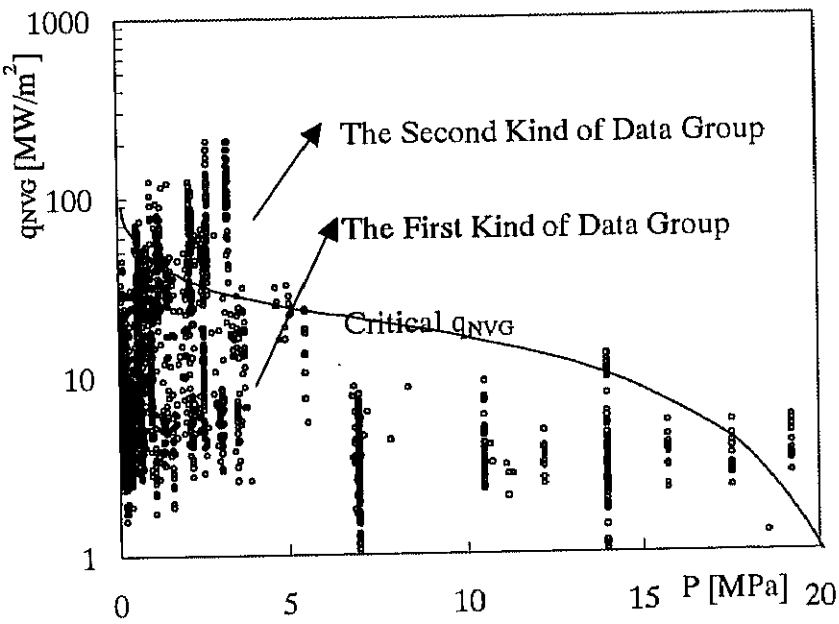

Fig.6-17 Categorization of the Data in the Appendix 1

One thing need specifying here is that, because the Thom correlation is only an empirical approximation, the critical q_{NVG} curve shown in Figs.6-16 and 6-17 is considered being only an approximation. Actually, some points near the curve with falling in the second kind of data group are found can be predicted quite well from the liquid sublayer dryout mechanism for the first kind of data group.

6.3.3 The CHF Prediction for the First Kind of Data Group

For the first kind of data group, which possesses q_{NVG} lower than the critical q_{NVG}, the CHF may be triggered either by the liquid sublayer dryout mechanism or the explosive-like film boiling and finally should be determined by the earlier happening one. If under the CHF calculated from the liquid sublayer dryout mechanism, the highest wall temperature has exceeded the homogenous nucleation temperature, the CHF then should be determined by q_{HN}, at which the highest wall temperature reaches the homogenous nucleation temperature. The relation between the q_{HN} and the pressure P is the same as the relation between the critical q_{NVG} and P shown in the fig.6-16 (but the meanings of the q_{HN} and the critical q_{NVG} are different). Otherwise, if under the CHF calculated from the liquid sublayer dryout mechanism, the highest wall temperature is still lower than the homogenous nucleation temperature, the CHF is then determined by the liquid sublayer dryout mechanism. The data that possess q_{NVG} lower than the critical q_{NVG} while with the CHF determined by the film boiling due to the establishment of the second kind of flow pattern is called in this paper as the third kind of data group. As mentioned above, in the totally 2482 data points, with the Levy (Ahmad) NVG model, predominant 2151 (2190) data possess a lower q_{NVG} than the critical q_{NVG} and fall in the region lower than the curve. In these 2151 (2190) data points, finally 122 (162) data points are found being determined by the happening of the film boiling. The data are all characterized by high mass flux, low L/D or high-pressure condition.

The data reported over prediction tendency in chapter 4 theoretically all fall in this third kind of data group. Under same low L/D value, because the T_{HN} is much easily reached at high pressure (as shown in fig.6-15), the CHF is therefore much easily determined by the occurrence of the film boiling. This is considered as the reason for the more obvious over-prediction tendency at high pressure.

Table 6-9 Comparisons of the CHF Predictions with Considering or Not Considering the Film Boiling Mechanism (for Low L/D Data, Total 283 Points)

Model \ Error Band		±5 (%)	±10 (%)	±15 (%)	±20 (%)	±25 (%)	±30 (%)	±35 (%)	±50 (%)	R.M.S (%)
χ_{Ahmad} α_{Ahmad}	With considering film boiling mechanism	13.43	23.67	30.39	37.81	44.17	53	58.66	73.5	49.49
	With no considering film boiling mechanism	13.07	21.55	26.5	33.57	37.81	45.23	49.47	57.24	94.95
χ_{Jafri} α_{Dix}	With considering film boiling mechanism	14.84	31.1	43.46	50.88	58.66	66.78	72.44	89.75	31.53
	With no considering film boiling mechanism	15.55	31.45	43.11	49.82	56.54	63.25	67.84	81.98	38.17

The comparison for the CHF prediction for the low L/D data is carried out with considering or not considering the film boiling mechanism and with employing the different model adoptions for the true quality and the void fraction. The effectiveness of the consideration of the film boiling mechanism can be got from the table 6-9 and fig.6-18.

Besides, as mentioned in the chapter 6.1, the employments of the more reasonable correlations for the true quality and the void fraction are also effective for the CHF prediction improvement for the low L/D data.

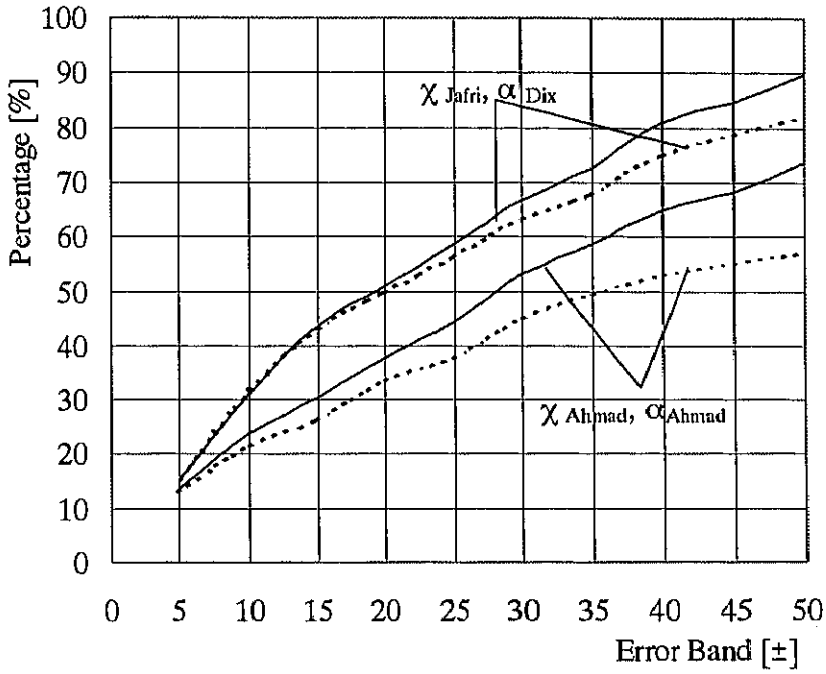

——— Considering the Film Boiling Mechanism

- - - - - - No Considering the Film Boiling Mechanism

Fig.6-18 Comparisons of the CHF Predictions with Considering or Not Considering the Film Boiling Mechanism for Low L/D Data

6.3.4 The CHF Prediction for the Second Kind of Data Group

As defined above, the second kind of data group is the data group that possesses a higher q_{NVG} than the critical q_{NVG} value. For such kind of data, the first kind of flow pattern cannot be established at all. The happening of the second kind of flow pattern itself is considered being the CHF triggering mechanism. The CHF is triggered by the high-density vapor bubbles accumulating at the interface between the wall and coolant due to the happening of homogeneous nucleation at the point where the wall temperature exceeds the homogenous nucleation temperature. The highest possible CHF is therefore restricted by the q_{NVG}, that is $CHF \le q_{NVG}$. The wall temperature distribution in the region before the NVG point is the key for the CHF prediction. But for the little knowledge for the heat transfer characteristics in the partial boiling region (region BC in fig.1-4), the accurate wall temperature prediction along the tube is still impossible at present. In the following, an approximation method is proposed for the CHF prediction for the second kind of data group.

As we know, the single-phase convective contribution works in both the single-phase flow (region AB in fig.1-4) and the partial boiling region (region BC). In these regions the tube is well wetted and the CHF is assumed to be difficult to happen. The CHF is assumed to happen much easily in the region CD where possesses the highest wall temperature with bubble still attaching to the tube wall. Therefore the lowest possible CHF for the second kind of data group is approximately assumed being restricted by the q_{FDB}, the heat flux for the establishment of FDB at the tube exit. Combined with the possible highest CHF, as discussed in the last paragraph, the CHF for the second kind of data group is restricted in the scope that:

$$q_{FDB} \le CHF \le q_{NVG}.$$

Because the points C and D are near to each other very much (fig.1-4), q_{FDB} then can be approximately assumed to be equal to the q_{NVG}. Then the CHF can be approximately written as:

$$CHF \approx q_{FDB} \approx q_{NVG}.$$

The method has been tested with Bortoli data (1958, for high pressure condition), Ornatsukii data (1965, 1960, for high G condition) and Mudarwar data (1999, for extremely high G or low L/D condition) with great success (Liu et al, 2000). As reported in the Chapter 4.1, for the data that originally cannot be predicted from the liquid sublayer dryout mechanism (accompanied by extremely high pressure or high mass flux), the CHF is finally calculated by doing a little modification to the vapor blanket equivalent diameter D_B (by increasing D_B step by step). With the modification, because the calculated CHF is actually the lowest possible CHF value (q_{NVG}), which is occasionally just the same as the analyzed CHF value, the CHF is therefore predicted successfully.

6.3.5 Summaries of the Triggering Mechanisms and Predictions for the Subcooled Flow Boiling CHF

With the above discussions, data are categorized into 3 groups. The first group is the data group that possesses q_{NVG} lower than the critical q_{NVG} and the CHF is determined by the liquid sublayer dryout mechanism. Predominant working conditions fall in this data group. The second group is the data group that possesses q_{NVG} higher than the critical q_{NVG} and the CHF is triggered due to the happening of the explosive-like film boiling. The third group is the data group that although possesses q_{NVG} lower than the critical q_{NVG} as the first kind of data group, the CHF is determined by the explosive-like film boiling due to the film boiling happens earlier than the CHF caused by the liquid sublayer dryout mechanism. The unpredictable points in the proposed liquid sublayer dryout model are found all falling in this data group while the over-prediction points is considered falling in the third kind of data group. The third kind of data group is a transition between the first and the second data group. The categorizing of the CHF triggering mechanism is summarized in table 6-10.

Theoretically, the CHF prediction for a random working condition should be:

1. Under a working condition, calculate q_{NVG};
2. Compare the q_{NVG} with the critical q_{NVG};
3. If $q_{NVG} \geq$ critical q_{NVG}, the CHF happens due to establishment of the second kind of flow pattern. The CHF is then determined by: $CHF = CHF_{Film\text{-}boiling} = q_{NVG}$.
4. If $q_{NVG} \leq$ critical q_{NVG}, calculate the CHF_{Dryout} from liquid sublayer dryout mechanism as introduced in chapter 3.

   (4a) If $CHF_{Dryout} < q_{HN}$, $CHF = CHF_{Dryout}$.

   (4b) Else if $CHF_{Dryout} \geq q_{HN}$, $CHF = CHF_{Film\text{-}boiling} = q_{HN}$.

Table 6-10 Summaries of the CHF Triggering Mechanisms

	For a certain working condition (G, P, D, L/D, T_{in}) with characteristic parameters q_{NVG} and q_{SAT}		
	if q_{NVG} < critical q_{NVG},		If $q_{NVG} \geq$ critical q_{NVG}
Data Categorizing	If $CHF_{Dryout} < q_{HN}$, The first kind of data group	If $CHF_{Dryout} \geq q_{HN}$, The third kind of data group	The second kind of data group
CHF triggering mechanism	The liquid sublayer dryout mechanism	The film boiling mechanism	The film boiling mechanism
CHF scope	$q_{NVG} \leq CHF_{Dryout} \leq q_{SAT}$	$q_{NVG} \leq CHF_{Film\text{-}boiling} \leq q_{SAT}$	$q_{FDB} \leq CHF_{Film\text{-}boiling} \leq q_{NVG}$
CHF	$CHF = CHF_{Dryout}$	$CHF = CHF_{Film\text{-}boiling} \approx q_{HN}$	$CHF = CHF_{Film\text{-}boiling} \approx q_{NVG}$
Working scope	Ordinary condition	Happens at high pressure or high heat flux (accompanied by low L/D, high G and low D) condition.	Easily happens at extremely high pressure or extremely high heat flux condition (accompanied by extremely high G; low D and low L/D)
Data distribution (Appendix 1, totally 2482 points)	2029	122	331

Actually, for the empirical of the Thom correlation, clear distinguish among the three kind of data group is still difficult. The CHF for a random given condition is therefore recommended to predict from:

(1) Calculate the CHF from the proposed liquid sublayer dryout mechanism

(2) If the CHF cannot be predicted, the CHF is calculated from the modification to the D_B, as introduced in chapter 4.1 (the second kind of data group).

(3) If the CHF can be predicted, calculate the CHF from the liquid sublayer dryout mechanism.

   (3a) If the $CHF_{Dryout} < q_{HN}$, $CHF = CHF_{Dryout}$ (the first kind of data group);

   (3b) Else if $CHF_{Dryout} \geq q_{HN}$, $CHF = q_{HN}$ (the third kind of data group).